Journal of Computational Physics **181,** 454–477 (2002)
doi:10.1006/jcph.2002.7137

Least-Squares Spectral Elements Applied to the Stokes Problem

M. M. J. Proot and M. I. Gerrtisma

Delft University of Technology, Aerospace Engineering, Section Aerodynamics, Kluyverweg 1, Delft, The Netherlands
E-mail: m.m.j.proot@lr.tudelft.nl, m.i.gerrtisma@lr.tudelft.nl

Received February 6, 2002; revised June 3, 2002

Least-squares spectral element methods are based on two important and successful numerical methods: spectral/*hp* element methods and least-squares finite element methods. In this respect, least-squares spectral element methods seem very powerful since they combine the generality of finite element methods with the accuracy of the spectral methods and also have the theoretical and computational advantages of the least-squares methods. These features make the proposed method a competitive candidate for the solution of large-scale problems arising in scientific computing. In order to demonstrate its competitiveness, the method has been applied to an analytical problem and the theoretical optimal and suboptimal a priori estimates have been confirmed for various boundary conditions. Moreover, the exponential convergence rates, typical for a spectral element discretization, have also been confirmed. The comparison with the classical Galerkin spectral element method revealed that the least-squares spectral element method is as accurate as the Galerkin method for the smooth model problem. © 2002 Elsevier Science (USA)

Key Words: least-squares; spectral elements; Stokes problem; a priori error analysis.

1. INTRODUCTION

Spectral element methods combine the generality of finite element methods with the higher order accuracy of the solution due to the high-order basis-functions [18]. Consequently, since these methods are often associated with high-order finite element methods, they are called *hp*-finite element methods [25]. In comparison with finite element methods, spectral element methods need fewer degrees of freedom to obtain a prescribed level of accuracy, but the amount of work that needs to be done per degree of freedom is higher. Since spectral element methods are a subclass of finite element methods, weak formulations for the spectral element method may be obtained by Galerkin's method.

0021-9991/02 $35.00

Recently, the spectral element discretization of the incompressible Navier–Stokes equations has received much attention [14, 25]. In the weak formulation, one needs to define approximating functional spaces for the velocity and pressure. However, the velocity and pressure cannot be approximated independently due to the well known Ladyzhenskaya–Babuška–Brezzi compatibility condition. This condition can be satisfied by reducing the polynomial order for the pressure. A well known compatible velocity–pressure combination is the so-called $P_N \times P_{N-2}$ formulation of Bernardi and Maday [4], [26]. The resulting discrete system is derived from a saddle point problem and is difficult to solve numerically. To overcome this, the discrete governing equations are often decoupled by using projection methods or generalized block LU-decompositions.

For many engineering flow problems, the least-squares principles offer several theoretical and computational advantages in the algorithmic design and implementation of the corresponding finite element methods that are not present in standard Galerkin-based discretization. In particular, the least-squares formulations for the Stokes equations [15, 22, 23] and Navier–Stokes equations [20, 24] lead to symmetric and positive definite algebraic systems and, additionally, circumvent the Ladyzhenskaya–Babuška–Brezzi stability condition. In the solution strategy of the incompressible Navier–Stokes equations, the least-squares principle can offer the following significant advantages: (1) one can use equal order interpolating polynomials for all the variables [6]; (2) the algebraic problems can be solved with robust iterative methods such as the preconditioned conjugate gradient (PCG) method [10]; (3) these methods can be implemented with an efficient element-by-element Jacobi–CG method which does not require the global assembly of the local matrices [9, 21] (an efficient matrix-free algorithm can be used in cases where storage is extremely limited [16]; (4) parallelization is straightforward by using element-by-element techniques [11]; and (5) in conjunction with a Newton linearization and a properly implemented continuation technique with respect to the Reynolds number, the solution technique will only involve symmetric positive definite linear systems [6]. A disadvantage of the least-squares methods is that the governing equations must be transformed into first-order systems to mitigate the continuity requirements between neighbouring finite elements and to keep the condition number of the resulting discrete system under control [3].

Least-squares spectral element methods (LSQSEM) seem very promising for the solution of large-scale problems arising in scientific computing, since these methods combine the generality of finite element methods with the accuracy of the spectral methods and also the theoretical and computational advantages in the algorithmic design and implementation of the least-squares methods (see Fig. 1). The first logical step in the development of least-squares spectral element methods for the incompressible Navier–Stokes equations consists of the development of efficient and accurate Stokes solvers.

Therefore, the main goals of the paper are threefold. After the discussion of the notations and definitions (Section 2), the first goal of the paper is treated, which is the discussion of the least-squares finite element method in the context of an abstract boundary value problem (Section 3). Secondly, this general formulation is subsequently applied to derive a least-squares spectral element formulation of the Stokes problem cast in velocity–vorticity–pressure form (Section 4). It is shown that the rate of convergence depends on the choice of the boundary condition when h-refinement is used. Finally, the (sub)optimal rate of convergence, predicted by the theory, is checked for a given model problem supplemented with various boundary conditions (Section 5). Moreover, all the results confirm the exponential rate of convergence when p-refinement is applied. Furthermore, a comparison with

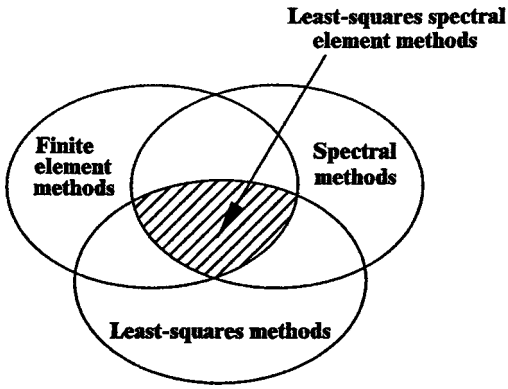

FIG. 1. The setting of least-squares spectral element methods. Best of all worlds?

the Galerkin spectral element method is also performed and the results discussed. The last section (Section 6) is devoted to conclusions.

2. NOTATION

In the remainder of this paper, vectors are denoted by boldface letters (e.g., **u**), and C denotes a generic positive constant whose meaning and value changes with the context. Let Ω denote an open bounded domain in $\mathbb{R}^n$, $n = 2$ or 3, with Lipschitz boundary Γ. On this boundary, **n** denotes the unit outward normal.

The space $L^p(\Omega)$, $1 \le p \le \infty$ represents the space of functions u for which the pth power of the absolute value is Lebesque integrable over the domain Ω. The associated norm is given by

$$\|u\|_{L^p(\Omega)} = \left(\int_\Omega |u|^p \, d\Omega \right)^{1/p}. \tag{1}$$

The space $H^0(\Omega) = L^2(\Omega)$ is a Hilbert space of square integrable functions defined over the domain Ω, equipped with the inner product

$$(u, v)_{0,\Omega} = \int_\Omega uv \, d\Omega \tag{2}$$

and norm

$$\|u\|^2_{L^2(\Omega)} = \|u\|^2_{0,\Omega} = (u, u)_{0,\Omega} = \int_\Omega u^2 \, d\Omega. \tag{3}$$

For some $m \ge 1$, the Sobolev spaces $H^m(\Omega)$ consist of square integrable functions u whose derivative up to order m are square integrable over the domain. The space $H^m(\Omega)$ is denoted by

$$H^m(\Omega) = \{u \in L^2(\Omega) : D^\alpha u \in L^2(\Omega), \text{ for } |\alpha| \le m\}, \tag{4}$$

where D^α represents the multi-index notation. The space $H^m(\Omega)$ is equipped with the inner product

$$(u, v)_{m,\Omega} = \sum_{|\alpha|\le m} (D^\alpha u, D^\alpha v)_{0,\Omega}, \tag{5}$$

and its associated norm

$$\|u\|^2_{m,\Omega} = (u, u)_{m,\Omega}. \tag{6}$$

When there is no ambiguity, the measure Ω is omitted from the inner product and norm definitions. When we use the $L^2(\Omega)$ space, the notation is further simplified by omitting the 0 subscript from the inner products and norms.

The inner products and norms are denoted for a vector-valued function of n components, belonging to the product space $\mathbf{X} = H^{m_1}(\Omega) \times \cdots \times H^{m_n}(\Omega)$, by $(\cdot,\cdot)_{\mathbf{x}}$ and $\|\cdot\|_{\mathbf{x}}$, respectively. When all the indices m_i are equal, the product space $\mathbf{X}$ is denoted by $[H^m(\Omega)]^n$ or $\mathbf{H}^m(\Omega)$, and $(\cdot,\cdot)_{m,\Omega}$ and $\|\cdot\|_{m,\Omega}$ are used for the notation of the inner products and norm.

The space $L^2_0(\Omega)$ consists of a square integrable function with zero mean with respect to the domain Ω. Finally, the space $H^m_0(\Omega)$ represents the closure of all infinitely differentiable functions with compact support in Ω, denoted by $\mathcal{D}(\Omega)$ in the H^m-norm. Furthermore, we define the spaces $H(\mathrm{div};\Omega)$ and $H(\mathrm{rot};\Omega)$ by

$$H(\mathrm{div};\Omega) = \{\mathbf{u} \in \mathbf{L}^2(\Omega) : \nabla\cdot\mathbf{u} \in L^2(\Omega)\} \tag{7}$$

and

$$H(\mathrm{rot};\Omega) = \{\mathbf{u} \in \mathbf{L}^2(\Omega) : \nabla\times\mathbf{u} \in \mathbf{L}^2(\Omega)\}. \tag{8}$$

The associated norms are

$$\|\mathbf{u}\|_{H(\mathrm{div};\Omega)} = \|\mathbf{u}\|_{L^2(\Omega)} + \|\nabla\cdot\mathbf{u}\|_{L^2(\Omega)} \tag{9}$$

and

$$\|\mathbf{u}\|_{H(\mathrm{rot};\Omega)} = \|\mathbf{u}\|_{L^2(\Omega)} + \|\nabla\times\mathbf{u}\|_{L^2(\Omega)}, \tag{10}$$

respectively. By $H_0(\mathrm{div};\Omega)$ and $H_0(\mathrm{rot};\Omega)$ we denote the closure of $\mathcal{D}(\Omega)$ in the $H(\mathrm{div};\Omega)$- and $H(\mathrm{rot};\Omega)$-norm, respectively. Likewise, we can define the spaces $H_0(\mathrm{div};\Omega)$ and $H_0(\mathrm{rot};\Omega)$ by

$$H_0(\mathrm{div};\Omega) = \{\mathbf{u} \in H(\mathrm{div};\Omega) : \mathbf{u}\cdot\mathbf{n} = 0 \text{ on } \Gamma\} \tag{11}$$

and

$$H_0(\mathrm{rot};\Omega) = \{\mathbf{u} \in H(\mathrm{rot};\Omega) : \mathbf{u}\times\mathbf{n} = \mathbf{0} \text{ on } \Gamma\}. \tag{12}$$

3. THE ABSTRACT FORMULATION OF LEAST-SQUARES METHODS

The principle of least-squares methods is first discussed for an abstract elliptic boundary value problem. An important aspect in theoretical analysis of least-squares formulations is to establish the equivalence between the residual of the differential equation in a certain norm and the error with respect to the exact solution in a corresponding norm. This equivalence is elaborated upon in Section 3.1. From the equivalence between the residual norm and the corresponding error norm, a priori error estimates can be derived. A general procedure based on the elliptic theory of Agmon, Douglus, and Nirenberg [1] provides this equivalence. Through the years, this theory has become known as the ADN theory.

Consider the abstract boundary value problem

$$\mathcal{L}(U) = F \quad \text{in } \Omega \tag{13}$$

$$\mathcal{R}(U) = G \quad \text{on } \Gamma, \tag{14}$$

in which $\mathcal{L}$ is a linear first-order partial differential operator acting on a scalar or vector U of unknowns, F is a given vector-valued function, $\mathcal{R}$ is a trace operator acting on the functions U, and G represents a given vector-valued function on the boundary. Without any loss of generality, one can take $G = 0$. If the governing equations involve second or higher order derivatives, the scalar equation or system will *first* be transformed into a first-order system. The reason for rewriting the system in an equivalent first-order system is to mitigate the continuity requirements between neighbouring spectral elements and to keep the condition number of the resulting discrete system under control [3].

3.1. Fully Coercive Least-Squares Methods with Strongly Imposed Boundary Conditions

It is assumed that the system given by (13)–(14) is well posed and that the operator $\mathcal{L}$ is a continuous mapping from the underlying function space X onto the space Y, i.e., there exists a positive constant M, independent of U, such that for all $U \in X$ the mapping $\mathcal{L}$ satisfies

$$\|\mathcal{L}(U)\|_Y \leq M\|U\|_X \quad \forall U \in X. \tag{15}$$

Additionally, we require that the mapping possess a continuous inverse, which can be expressed by

$$\alpha\|U\|_X \leq \|\mathcal{L}(U)\|_Y \quad \forall U \in X, \tag{16}$$

where α is a positive constant independent of U. The space X consists of functions which already satisfy the boundary condition (14) with $G = 0$. Note that by virtue of the estimate (15) and (16), the norms $\|\mathrm{U}\|_X$ and $\|\mathcal{L}(U)\|_Y$ are equivalent. The coercivity relation (16) is of paramount importance for the minimizing principle of least-squares methods. To appreciate this, assume that the function $U - U_e$ is measured by means of the estimate (16) where $U_e \in X$ represents the "exact" solution of the boundary value problem (13)–(14). Since $\mathcal{L}$ is a linear operator, and since U_e represents the exact solution, the estimate (16) can be recast into

$$\alpha\|U - U_e\|_X \leq (\|\mathcal{L}(U) - F\|_Y), \quad \forall U \in X. \tag{17}$$

This lower bound leads to the very important observation that if the norm of the residual of (13) approaches zero ($\|\mathcal{L}(U) - F\|_Y \to 0$), the approximate solution converges to the exact solution ($\|U - U_e\|_X \to 0$). Consequently, the unique minimizer of the quadratic least-squares functional,

$$\mathcal{I}(U) = \frac{1}{2}\left(\|\mathcal{L}(U) - F\|_Y^2\right), \quad \forall U \in X, \tag{18}$$

solves the boundary value problem (13)–(14). The minimization of the quadratic least-squares functional (18) written as

$$\text{Seek } U \in X \text{ such that } \mathcal{I}(U) \leq \mathcal{I}(V), \quad \forall V \in X \tag{19}$$

can be obtained by means of the Euler–Lagrange equation

$$\delta\mathcal{I}(U) = \lim_{\epsilon \to 0} \frac{d}{d\epsilon}\mathcal{I}(U + \epsilon V) = 0, \quad \forall V \in X \tag{20}$$

applied to the quadratic least-squares functional (18), which results in the weak formulation

$$\text{Seek } U \in X \text{ such that } B(U, V) = F(V), \quad \forall V \in X, \tag{21}$$

where $B(U, V) = (\mathcal{L}(U), \mathcal{L}(V))$ and $F(V) = (F, \mathcal{L}(V))$. Since $\mathrm{B}(\cdot,\cdot)$ is symmetric, continuous, and coercive in X by relation (16), and since $F(\cdot)$ is continuous, the weak formulation (21) has a unique solution by virtue of the Lax–Milgram lemma.

The last step in the derivation of the abstract boundary value problem consists of choosing a suitable finite-dimensional subspace $X^h \subset X$ which yields the discrete variational problem

$$\text{Seek } U^h \in X^h \text{ such that } B(U^h, V^h) = F(V^h), \quad \forall V^h \in X^h, \tag{22}$$

where the parametrized h presents a grid parameter (h is the mesh spacing for finite element methods or the reciprocal of the polynomial degree of spectral methods). In the present work, only conforming discretizations are considered.

3.2. Practicality and Optimality of Least-Squares Formulations

From a practical point of view, least-squares formulations which allow the use of C^0-finite or spectral elements are desirable [26a, 26b, 26c], but not necessary [17a]. This can be accomplished by *first* transforming the system into a first-order system and subsequently requiring that only (scaled) L^2-norms be used in the quadratic least-squares functional. Obvious choices for the function spaces X and Y are H^1- and L^2-spaces, respectively. Moreover, if one can prove that these spaces are equivalent, then the system exhibits some optimal properties. These optimal formulations are called *fully H^1-coercive* and can be very attractive.

In a finite element context, these optimal properties are reflected by an optimal rate of convergence in the H^0- and the H^1-norms. If the exact solution is $U_e \epsilon H^s(\Omega)$ for some $s \geq 2$, then the error estimates (see [27] for the mathematical details)

$$\|U_e - U^h\|_r \leq Ch^{l+1-r}\|U_e\|_{l+1} \quad r = 0, 1 \tag{23}$$

hold, where $l = \min(k, s-1)$ and where k represents the approximating order of the C^0-finite elements. The rate of convergence (23) provides the highest possible rate of convergence allowed by the polynomial order k. Note that the optimal rate of convergence depends on the polynomial degree (k) and the regularity of the exact solution (s). Since this rate of convergence arises from h-refinement, it is called h-convergence hereafter.

In a spectral element context, the approximating functions are algebraic polynomials of degree less than or equal to N in each variable. Typical for spectral element discretizations is that the rate of convergence is only bounded by the smoothness degree of the solution and not by any other grid parameter [27]. As a consequence, exponential convergence rates can be obtained for smooth problems if a p-refinement strategy is used. Since this rate of convergence results from p-refinement, it is called p-convergence hereafter. Moreover, since the p-convergence rates are exponential and thus already optimal compared to the finite element discretizations, it makes no sense to speak about optimal p-convergence rates. One can only check its exponential convergence behaviour.

4. THE LEAST-SQUARES SPECTRAL ELEMENT FORMULATION OF THE STOKES PROBLEM

4.1. The First-Order Formulation of the Stokes Problem

In the present paper, the two-dimensional Stokes problem will is considered. In order to obtain a *bona fide* least-squares formulation, the Stokes problem is *first* transformed into a system of first-order partial differential equations by introducing the vorticity as an auxiliary variable. By using the identity $\nabla \times \nabla \times u = -\Delta u + \nabla(\nabla \cdot \mathbf{u})$ and by using the incompressibility constraint $\nabla \cdot \mathbf{u} = 0$, the governing equations subsequently read

$$\nabla p + \nu \nabla \times \omega = \mathbf{f} \quad \text{in } \Omega \tag{24}$$

$$\omega - \nabla \times \mathbf{u} = 0 \quad \text{in } \Omega \tag{25}$$

$$\nabla \cdot \mathbf{u} = 0 \quad \text{in } \Omega, \tag{26}$$

where, in the particular case of the two-dimensional problem, $\mathbf{u}^T = [u_1, u_2]$ represents the velocity vector, p is the pressure, ω is the vorticity (i.e., the x_3-component of the vorticity vector), $\mathbf{f}^T = [f_1, f_2]$ is the forcing term per unit mass (if applicable), and ν is the kinematic viscosity. For simplicity it is further assumed that the density equals $\rho = 1$. In two dimensions, system (24)–(26) consists of four equations and four unknowns and is uniformly elliptic of order four. The linear Stokes operator and its right-hand side read

$$\mathcal{L}(U) = F \Leftrightarrow \begin{bmatrix} 0 & 0 & \nu\frac{\partial}{\partial x_2} & \frac{\partial}{\partial x_1} \\ 0 & 0 & -\nu\frac{\partial}{\partial x_1} & \frac{\partial}{\partial x_2} \\ \frac{\partial}{\partial x_2} & -\frac{\partial}{\partial x_1} & 1 & 0 \\ \frac{\partial}{\partial x_1} & +\frac{\partial}{\partial x_2} & 0 & 0 \end{bmatrix} \begin{bmatrix} u_1 \\ u_2 \\ \omega \\ p \end{bmatrix} = \begin{bmatrix} f_1 \\ f_2 \\ 0 \\ 0 \end{bmatrix} \quad \text{in } \Omega. \tag{27}$$

4.2. The Boundary Conditions

The two-dimensional Stokes problem (24)–(26) must be supplemented with a combination of the boundary conditions listed in Table I. The boundary conditions involve a

TABLE I
The Homogeneous Boundary Conditions of the Stokes Problem

Boundary conditions	2D implementation
Bc 1: Symmetry plane	$\mathbf{n}\cdot\mathbf{u}=0$
	$\omega=0$
Bc 2: Inflow	$\mathbf{n}\cdot\mathbf{u}=0$
	$p=0$
Bc 3: Outflow	$\mathbf{n}\times\mathbf{u}=0$
	$p=0$
Bc 4: Outflow	$\mathbf{n}\times\mathbf{u}=0$
	$\omega=0$
Bc 5: Wall, outflow	$\mathbf{n}\cdot\mathbf{u}=0$
	$\mathbf{n}\times\mathbf{u}=0$
Bc 6: Outflow	$\omega=0$
	$p=0$

combination of the normal velocity component, the tangential velocity component, pressure, and vorticity. Jiang [21] has shown that six boundary conditions can be used for the Stokes and Navier–Stokes equations.

Effectively, the homogeneous boundary value problem can be translated into the function spaces defined above. The six boundary conditions are:

- Bc 1: Find $(\mathbf{u}, \omega, p) \in H_0(\text{div}; \Omega) \cap H(\text{rot}; \Omega) \times H_0^1(\Omega) \times H^1(\Omega) \cap L_0^2(\Omega)$;
- Bc 2: Find $(\mathbf{u}, \omega, p) \in H_0(\text{div}; \Omega) \cap H(\text{rot}; \Omega) \times H^1(\Omega) \times H_0^1(\Omega)$;
- Bc 3: Find $(\mathbf{u}, \omega, p) \in H(\text{div}; \Omega) \cap H_0(\text{rot}; \Omega) \times H^1(\Omega) \times H_0^1(\Omega)$;
- Bc 4: Find $(\mathbf{u}, \omega, p) \in H(\text{div}; \Omega) \cap H_0(\text{rot}; \Omega) \times H_0^1(\Omega) \times H^1(\Omega) \cap L_0^2(\Omega)$;
- Bc 5: Find $(\mathbf{u}, \omega, p) \in \mathbf{H}_0^1(\Omega) \times H^1(\Omega) \times H^1(\Omega) \cap L_0^2(\Omega)$; and
- Bc 6: Find $(\mathbf{u}, \omega, p) \in \mathbf{H}^1(\Omega) \times H_0^1(\Omega) \times H_0^1(\Omega)$.

So instead of proving coercivity with respect to certain boundary conditions we can also consider the problem of obtaining coercivity with respect to the above function spaces, which already contain the prescribed homogeneous boundary conditions. This idea is elaborated upon in the next section.

4.3. A Priori Estimates and Least-Squares Functionals

The role of the boundary conditions in the least-squares formulation of the Stokes problem cast in the velocity–pressure–vorticity formulation reaches further than one would imagine at first glance. In order to obtain the *a priori error estimates* for the Stokes problem, the ADN [1] theory and in particular the *complementing condition* of the ADN theory are of paramount importance. The complementing condition is an algebraic condition on the principal parts of the differential equations and the boundary operators which guarantees the compatibility of a particular set of boundary conditions with the given system of differential equations. This condition is necessary and sufficient for the coercivity estimates to be valid (see [1, 5] for further details). Analyses based on the ADN theory revealed that the coercivity estimates for the Stokes operator (27) are not unique and depend on the choice

of the boundary conditions! Consequently, the rate of h-convergence of the least-squares formulation depends on the choice of the boundary conditions.

Jiang [21] has shown that for the boundary conditions Bc 1 to Bc 4 and Bc 6 of Table I the following coercivity relation of the Stokes differential operator holds:

$$\|\mathbf{u}\|_1 + \|\omega\|_1 + \|p\|_1 \leq C(\|\nabla p + \nu \nabla \times \omega\|_0 + \|\nabla \cdot \mathbf{u}\|_0 + \|\omega - \nabla \times \mathbf{u}\|_0). \tag{28}$$

Recently, Bochev and Gunzburger [5] pointed out that the relation (28) does not hold when using the velocity boundary conditions (Bc 5). Instead, one should use

$$\|\mathbf{u}\|_2 + \|\omega\|_1 + \|p\|_1 \leq C(\|\nabla p + \nu \nabla \times \omega\|_0 + \|\nabla \cdot \mathbf{u}\|_1 + \|\omega - \nabla \times \mathbf{u}\|_1). \tag{29}$$

In response to this observation, Jiang [21] argued that when the residuals of the Stokes equations supplemented with the velocity boundary conditions are measured with (non-scaled) H^0-norms, the variables must be measured in less desirable norms, and that the corresponding bounded below condition is now given by

$$\|\mathbf{u}\|_1 + \|\omega\|_0 + \|p\|_0 \leq C(\|\nabla p + \nu \nabla \times \omega\|_0 + \|\nabla \cdot \mathbf{u}\|_0 + \|\omega - \nabla \times \mathbf{u}\|_0). \tag{30}$$

Relations (28) and (30) yield the quadratic least-squares functional

$$\mathcal{I}(U) = \frac{1}{2}\big(\|\nabla p + \nu \nabla \times \omega - \mathbf{f}\|_0^2 + \|\nabla \cdot \mathbf{u}\|_0^2 + \|\omega - \nabla \times \mathbf{u}\|_0^2\big), \tag{31}$$

which upon minimization, yields a weak formulation which can be discretized with standard finite or spectral elements. This results from the fact that, since the norms in (31) must be square integrable in the domain, one can use C^0-finite or spectral elements. The quadratic least-squares functional resulting from relation (29) is given by

$$\mathcal{I}(U) = \frac{1}{2}\big(\|\nabla p + \nu \nabla \times \omega - \mathbf{f}\|_0^2 + \|\nabla \cdot \mathbf{u}\|_1^2 + \|\omega - \nabla \times \mathbf{u}\|_1^2\big). \tag{32}$$

Unfortunately, the appearance of the H^1-norms in (32) makes this functional not very practical since it would lead to the use of impractical C^1-finite or spectral elements for the velocity unknowns which require continuous first-order derivatives across interelement boundaries. The pressure and vorticity, in this formulation, can still be treated by standard C^0 elements. Instead, one can (based on scaling arguments between the discrete H^0- and H^1-norms [5, 13, 27]) minimize the weighted functional

$$\mathcal{I}(U) = \frac{1}{2}\big(\|\nabla p + \nu \nabla \times \omega - \mathbf{f}\|_0^2 + h^{-2}\|\nabla \cdot \mathbf{u}\|_0^2 + h^{-2}\|\omega - \nabla \times \mathbf{u}\|_0^2\big), \tag{33}$$

which leads to a weak formulation where again standard finite and spectral elements can be used. The parameter $h > 0$ represents a characteristic length of the grid which decreases when the size of the spectral element decreases or when the polynomial order increases. As observed in [6], the functionals (32) and (33) are only equivalent if the functions $\mathbf{u}$, ω, and p are restricted to finite-dimensional spaces. However, the functional (33) is no longer coercive in the usual sense. It was shown in [6] that in order to obtain an optimal accurate h-method, one needs to approximate the pressure and vorticity with an approximating polynomial of one order less than the order of the velocity-approximating polynomial. Consequently, a

TABLE II

The Various Least-Squares Formulations for the Stokes Problem Resulting from the General Least-Squares Functional $\mathcal{I}(U) = \frac{1}{2}(\mathbf{h}^a \|\nabla p + \nu\nabla \times \omega - \mathbf{f}\|_0^2 + h^b \|\nabla \cdot \mathbf{u}\|_0^2 + h^c \|\omega - \nabla \times \mathbf{u}\|_0^2)$

Boundary conditions	Values of coefficients a, b, and c	Norms of variables	Optimality of formulation
1. Symmetry plane	$a=0, b=0, c=0$	$\|\mathbf{u}\|_1, \|\omega\|_1, \|p\|_1$	Optimal
2. Inflow	$a=0, b=0, c=0$	$\|\mathbf{u}\|_1, \|\omega\|_1, \|p\|_1$	Optimal
3. Outflow	$a=0, b=0, c=0$	$\|\mathbf{u}\|_1, \|\omega\|_1, \|p\|_1$	Optimal
4. Outflow	$a=0, b=0, c=0$	$\|\mathbf{u}\|_1, \|\omega\|_1, \|p\|_1$	Optimal
5a. Wall, outflow	$a=0, b=0, c=0$	$\|\mathbf{u}\|_1, \|\omega\|_0, \|p\|_0$	Suboptimal
5b.	$a=0, b=-2, c=-2$	$\|\mathbf{u}\|_2, \|\omega\|_1, \|p\|_1$	Suboptimal
6. Outflow	$a=0, b=0, c=0$	$\|\mathbf{u}\|_1, \|\omega\|_1, \|p\|_1$	Optimal

suboptimal rate of h-convergence for the pressure and vorticity will be obtained when an equal-order interpolation is used for all the dependent variables. The velocity components should still converge at an optimal rate.

Table II summarizes the relation between the boundary conditions and the associated least-squares formulation. Column one lists the type of boundary condition; in column two the power of the scaling parameters is summarized; column three and four respectively indicate the norms in which the variables are measured and the optimality of the least-squares h-convergence rates for the pressure and vorticity when an equal-order interpolation for all variables is used. All formulations are cast into the general quadratic least-squares functional

$$\mathcal{I}(U) = \frac{1}{2}\left(\mathbf{h}^a \|\nabla p + \nu\nabla \times \omega - \mathbf{f}\|_0^2 + h^b \|\nabla \cdot \mathbf{u}\|_0^2 + h^c \|\omega - \nabla \times \mathbf{u}\|_0^2\right), \tag{34}$$

which upon minimization lead to the bilinear form

$$B(U, V) = \int_\Omega [\mathcal{L}(U)]^T W [\mathcal{L}(V)]\, d\Omega \tag{35}$$

and the linear functional

$$F(V) = \int_\Omega [F]^T W [\mathcal{L}(V)]\, d\Omega, \tag{36}$$

respectively. In (35) and (36), $[\ ]^T$ represents the transpose and W is a diagonal matrix with positive diagonal elements $[\mathbf{h}^a, h^b, h^c]$.

Inspection of Table II reveals that boundary conditions 1 to 4 and boundary condition 6 yield an optimal rate of h-convergence in all variables if an equal-order interpolant is used for all variables. This optimal property results from the fully H^1-coercive formulation. However, formulations 5a and 5b are not fully H^1-coercive. Consequently, when an equal-order approximation is used, the velocity component will still have an optimal rate of h-convergence, whereas the vorticity and pressure will have a suboptimal rate.

4.4. Implementational Aspects

Most spectral element methods are based on the Gauss–Lobatto–Legendre (GLL) numerical integration for reasons of efficiency [25]. The GLL integration of a function $f(\xi)$ on the interval $\xi \in [-1, 1]$ is given by

$$\int_{-1}^{1} f \, d\xi \approx \sum_{i=0}^{N} f(\xi_i) w_i, \tag{37}$$

where ξ_i and w_i represent the position and weight of the collocation point i of the one-dimensional Gauss–Lobatto–Legendre grid, respectively. The GLL collocation points are the roots of $(\xi^2 - 1)\frac{dL_N(\xi)}{d\xi}$, where $L_N(\xi)$ is the Legendre function of order N. Due to the choice of the numerical GLL-integration, the orthogonal discrete basis functions for the unknowns are readily available by means of the Lagrangian interpolants $h_i(\xi)$, with $0 \leq i \leq N$, defined on the interval $[-1, 1]$ by

$$h_i(\xi) = \frac{(\xi^2 - 1)\frac{dL_N(\xi)}{d\xi}}{N(N+1)L_N(\xi_i)(\xi - \xi_i)}. \tag{38}$$

Consequently, the approximation of a function $f(\xi)$ on the interval $[-1, 1]$ by using the Lagrangian interpolants reads

$$\tilde{f}(\xi) = \sum_{i=0}^{N} f(\xi_i) h_i(\xi), \tag{39}$$

where $f(\xi_i)$ is the value of the function $f(\xi)$, evaluated at the collocation point ξ_i; the function $h_i(\xi)$ represents the corresponding Lagrangian interpolant.

In multiple dimensions, the integration and basis functions can be obtained by means of tensor products. Since the numerical integration is only defined on the domain $[-1, 1]^d$ (where d represents the spatial dimension), one needs a mapping from a general element (a quadrilateral in 2D) onto the *master* or *parent* element. The order of the spectral elements (N) refers to the order of the Legendre function which is used for the GLL integration and Lagrangian interpolants.

In the present paper, the domain has been discretized with a mesh of nonoverlapping conforming quadrilateral spectral elements of order N which are used to solve the two-dimensional Stokes problem (24)–(26). Each quadrilateral spectral element is mapped on the parent spectral element Ω_e by using an isoparametric mapping [19] to the bi-unit square $[-1, 1] \times [-1, 1]$ with local coordinates ξ_1 and ξ_2. In the parent element all variables, located at the GLL collocation points, can be approximated by the same Lagrangian interpolant, since the least-squares formulation is not constrained by the Ladyzhenskaya–Babuška–Brezzi compatibility condition. For the two-dimensional Stokes problem, the discrete spectral element approximation yields

$$\mathbf{U}^h = \sum_{q=0}^{N} \sum_{p=0}^{N} h_p(\xi_1) h_q(\xi_2) \begin{bmatrix} \hat{u}_1 \\ \hat{u}_2 \\ \hat{\omega} \\ \hat{p} \end{bmatrix}_{p,q}, \tag{40}$$

where $h_p(\xi_1)$ with $0 \le p \le N$ and $h_q(\xi_2)$ with $0 \le q \le N$ represent the Lagrange interpolants in the ξ_1 and ξ_2 direction, respectively. The vector $[\hat{u}_1, \hat{u}_2, \hat{\omega}, \hat{p}]^T$ in (40) is the vector of unknown coefficients, evaluated at the collocation point. The global assembling of the element matrices

$$K_e = \int_{\Omega_e} [\mathcal{L}(\psi_{0,0}), \ldots, \mathcal{L}(\psi_{N,N})]^T W [\mathcal{L}(\psi_{0,0}), \ldots, \mathcal{L}(\psi_{N,N})] \, d\Omega, \tag{41}$$

where $\psi_{p,q} = h_p(\xi_1) h_q(\xi_2)$ with the element right-hand sides

$$F_e = \int_{\Omega_e} [\mathcal{L}(\psi_{0,0}), \ldots, \mathcal{L}(\psi_{N,N})]^T W F \, d\Omega, \tag{42}$$

yields the global assembled system of linear algebraic equations

$$KU = F, \tag{43}$$

where U now represents the global vector of unknown nodal values. The matrix W represents a diagonal matrix as defined in Section 4.3. Note that since the matrix K is symmetric positive definite, robust preconditioned conjugate gradient iterative methods can be employed and that no extra added weighting (e.g., tuning) parameters have to be introduced in the least-squares spectral element formulation.

5. NUMERICAL RESULTS

The purpose of the numerical simulations is threefold. First of all, we want to establish the optimal h-convergence rates for least-squares spectral element methods. Secondly, we want to check the exponential p-convergence rates of these methods. Finally, we want to compare the accuracy and the convergence rates of the least-squares spectral element method with those obtained through the Galerkin spectral element method. To this end, the h- and p-convergence rates are calculated for a model problem supplemented with inflow and velocity boundary conditions. One of the *tricky* properties of least-squares methods is that they can solve overdetermined problems. As an example, the model problem is solved with overdetermined but consistent boundary conditions. Also for this latter test case, the h- and p-convergence rates are investigated. All simulations are obtained by using equal-order interpolation polynomials for implementational reasons (ease of programming).

5.1. The Model Problem

The h- and p-rate of convergence of the least-squares spectral element formulation of the velocity–vorticity–pressure formulation of the Stokes problem is demonstrated by means of the model problem of Gerritsma and Phillips [17] with $\nu = 1$. This model problem involves an exact solution of the Stokes problem where the velocity components and pressure are defined on the unit square $[0, 1] \times [0, 1]$ by

$$U(x, y) = -\sin(2\pi x)\cos(2\pi y) \tag{44}$$

$$V(x, y) = \cos(2\pi x)\sin(2\pi y) \tag{45}$$

and

$$P(x, y) = \sin(\pi x)\sin(\pi y), \tag{46}$$

where $U(x, y)$ and $V(x, y)$ represent the velocity in the x and y direction, respectively; the vorticity is derived from the velocity components. This exact solution satisfies the Stokes equations if the following forcing term is used:

$$\mathbf{f} = \begin{pmatrix} \pi \cos(\pi x) \sin(\pi y) - 8\pi^2 \sin(2\pi x) \cos(2\pi y) \\ \pi \sin(\pi x) \cos(\pi y) + 8\pi^2 \cos(2\pi x) \sin(2\pi y) \end{pmatrix}. \tag{47}$$

5.2. The Test Cases

As a first test case, the model Stokes problem is solved with the homogeneous boundary condition 2 (Bc 2) of Table I. For this test case, the normal components of the velocity and the pressure are prescribed on the boundary ($p = 0, \mathbf{n} \cdot \mathbf{u} = 0$). For the second test case, the two inhomogeneous velocity components, given by Eqs. (44) and (45), are prescribed on the boundary. The pressure constant is set to zero in the point (0, 0). The model problem supplemented with the inhomogeneous velocity boundary condition is solved in least-squares sense for formulations 5a and 5b. Recall that the difference between the formulations is the scaling parameter h^2 which is defined in the present paper as the area of the spectral element divided by N^2. For the last test case, an overdetermined but consistent problem is solved with a boundary where all the variables are prescribed. The interest for this test case is to obtain insight into the convergence behaviour for overdetermined least-squares formulations since a similar boundary condition strategy may facilitate the extension of the present least-squares spectral element methods to discontinuous least-squares spectral element methods [17a] and/or methods with hp-adaptive strategies.

5.3. The h-Convergence Results

Six different grids have been used to check the optimal properties of the h-convergence rates. As can be observed in Table III, the polynomial order of all the spectral elements equals 4, and the number of spectral elements was varied from 9 to 64. Three grids that were used in the simulation are shown in Fig. 2. For each grid of Table III, the numerical solutions obtained for each test case are compared with the exact solution. To this end, the

TABLE III
The Various Grids Used for the Investigation of the h-Convergence Rates

Spectral elements	Approximating order
9	4
16	4
25	4
36	4
49	4
64	4

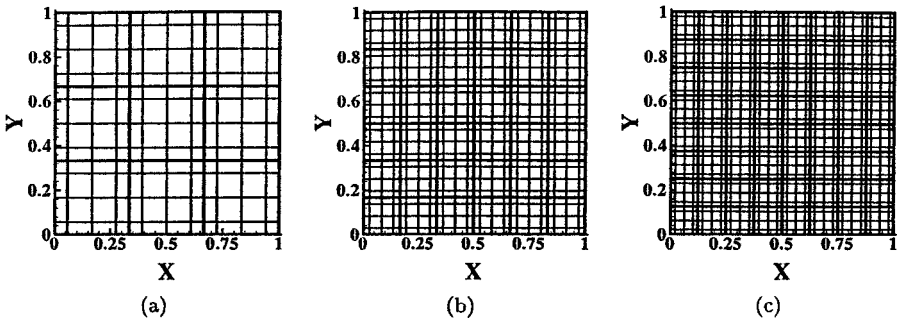

FIG. 2. Three examples of the numerical grids used for the calculation of the h-convergence rates (left: a GLL grid with 9 spectral elements of order 4; center: a GLL grid with 36 spectral elements of order 4; right: a GLL grid with 64 spectral elements of order 4).

error between the exact and the computed solution is obtained by means of H^0 and H^1 norms. We refer to these norms as the *error norms*. In the present paper, all the norms are calculated by using the numerical Gauss–Legendre–Lobatto integration of order 20. The h-convergence rates of the H^0 and H^1 error norms are displayed as a function of the grid parameter h in Figs. 3 and 4, respectively.

It can be observed in Figs. 3a and 4a that the U-velocity components converge at approximately the same optimal rate for all the test cases. The values of the H^0 and H^1 error norms of the nonweighted least-squares formulation (formulation 5a) seem a little larger on the coarser grids but recover the same values as the other test cases on the finest grids.

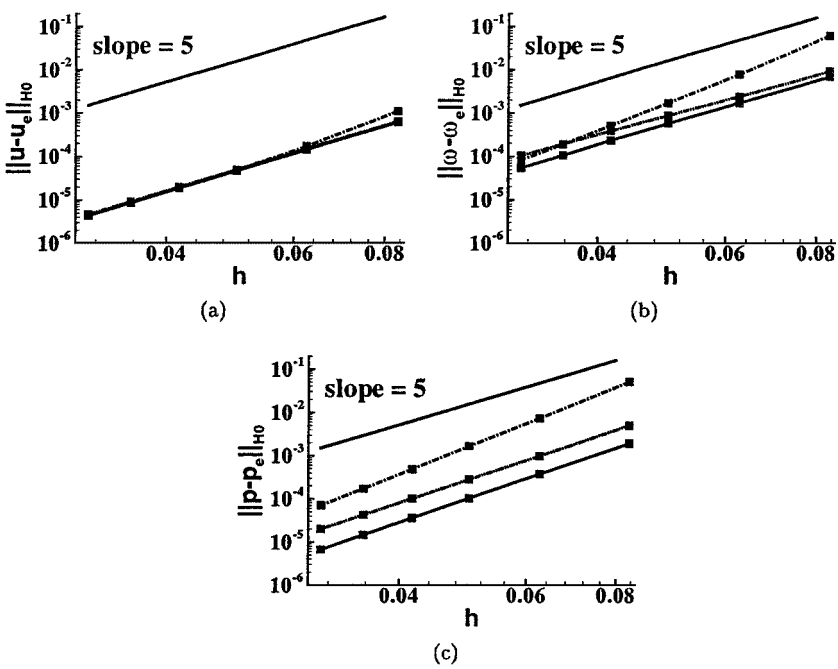

FIG. 3. The h-convergence rate of the H^0 error norms for the different test cases (Bc 2: -; Overdet. Bc: - -; Bc 5a:·-·; and Bc 5b:·---·).

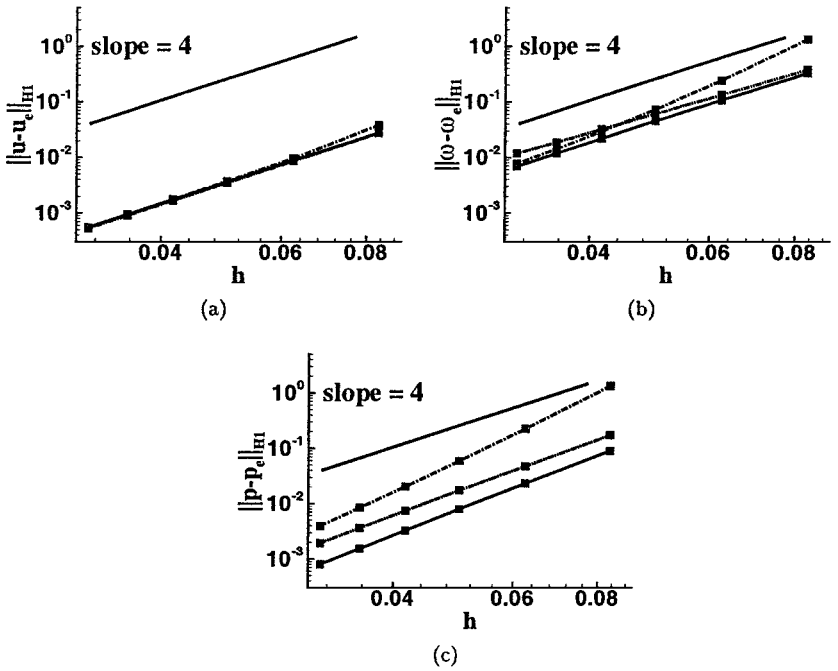

FIG. 4. The h-convergence rate of the H^1 error norms for the various test cases (Bc 2: -; Overdet. Bc:- -; Bc 5a:-·-; and Bc 5b:-···).

Consequently, the rate of h-convergence of formulation 5a will be slightly higher than it is for the other test cases. All the convergence rates of the H^0 and H^1 error norms are summarized in Table IV. In this table one can observe that formulation 5a converges at a higher than optimal rate. All the other formulations converge at the optimal rate. Further scrutiny of the data revealed the scatter in the data of formulation 5a. This might partly explain the overprediction of the rate of convergence caused by the linear regression used. Comparing formulation 5a (nonweighted formulation) and 5b (weighted formulation) indicates that weighting has a positive effect on the smoothness of the h-convergence rates. The results further indicate that the use of the overdetermined but consistent boundary condition yields an optimal convergence behaviour for the U-velocity component. Since the result of the V-velocity component yields a convergence rate similar to that of the U-velocity component, it is not shown in Figs. 3 and 4.

TABLE IV
Summary of the h-Convergence Rates in the H^0 and H^1 Error Norms for the Model Problem

	The H^0 error norms				The H^1 error norms			
Function	Bc 2	OD	Bc 5a	Bc 5b	Bc 2	OD	Bc 5a	Bc 5b
U	5.02	5.02	5.09	5.01	4.00	4.00	4.04	4.00
V	5.02	5.02	5.09	5.01	4.00	4.00	4.04	4.00
ω	4.99	4.99	6.10	4.42	3.99	3.99	4.60	3.52
P	5.86	5.86	6.81	5.69	4.91	4.91	5.72	4.67

In Figs. 3b and 4b, the h-convergence rate of the vorticity can be found. It can be observed in these figures that the inflow boundary condition and the overdetermined boundary condition yield optimal h-convergence rates in the H^0 and H^1 error norms, respectively. Since the error norms of these formulations are on top of each other, one can only see the full line corresponding to the inflow boundary condition. As predicted by the error estimates, formulation 5b reveals a suboptimal h-convergence rate in both the H^0 and H^1 error norms. The h-convergence behaviour of formulation 5a (nonweighted formulation) is unexpected since the H^0 and H^1 error norms converge at a rate which is higher than the optimal h-convergence rate! Investigation of Figs. 3b and 4b reveals that the overprediction of the h-convergence rate cannot result only from the linear regression used to calculate the convergence rates. We have never seen such convergence behaviour (at least not to this extent) and have no explanation for it. It seems that for formulation 5a, the behaviour of the vorticity resembles the behaviour of the U-velocity component. Although the rate of h convergence of formulation 5a is better than optimal, the absolute values of the H^0 and H^1 error norms are still larger than those of the optimal formulations.

Figures 3c and 4c display the h-convergence rates in the H^0 and H^1 error norms of the pressure. As can be observed in Figs. 3c and 4c and in Table IV, all rates are better than the optimal rate of convergence Comparing the results obtained with the inflow boundary condition to those obtained with the overdetermined boundary condition reveals that the convergence rate and the absolute values of the H^0 and H^1 error norms are equal (e.g., the lines fall on top of each other). The rate of convergence and the accuracy of formulation 5b are suboptimal compared to the previous two cases. For these three cases, the difference between the h-convergence rate of the H^0 and H^1 error norms is almost 1 (as it should be)!

From these results it can be concluded that the velocity components are most accurate and that the H^0 and H^1 error norms converge at an optimal rate for all the boundary conditions tested. Indeed, the overdetermined boundary condition also yields optimal accurate results! Moreover, the accuracy of the pressure variable is less than one order worse than the accuracy of the velocity components and converges at a rate which is higher than the optimal h-convergence rate. Further experiments with least-squares spectral element methods will, we hope, clarify whether this phenomenon is model problem dependent or a general trend for higher order methods. The vorticity values are the least accurate. In general, the H^0 and H^1 error norms are one order of magnitude higher than the H^0 and H^1 error norms for the velocity and converge according to the error estimates. The convergence behaviour of formulation 5a is very unpredictable and requires fine meshes to obtain accurate results for the pressure and vorticity.

5.4. The p-Convergence Results

The recent interest in and demand for more accurate and at the same time geometrical, flexible methods resulted in the development of spectral element methods [25]. As stated above, an important aspect of spectral element methods is the exponential rate of convergence obtainable when p-refinement is applied. In order to investigate the exponential p-convergence rate of the least-square formulations, four p-grids have been used to simulate the model problem for all the test cases. Each grid contains four spectral elements. The order of the approximating polynomial varied from 4 to 10 in steps of 2 and was the

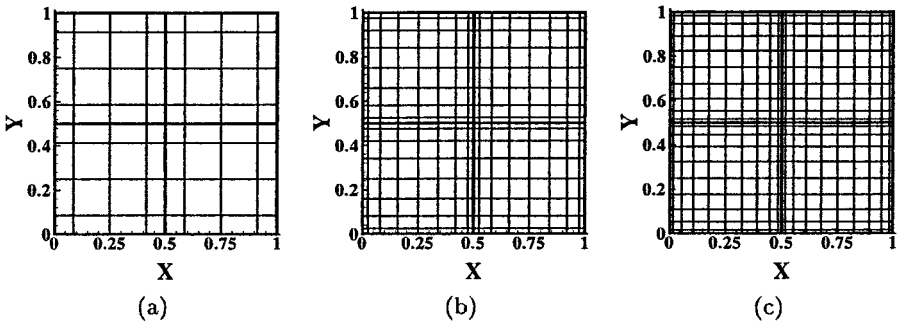

FIG. 5. Three examples of the numerical grids used for the calculations (left: a GLL grid with four spectral elements of order 4; center: a GLL grid with four spectral elements of order 8; right: a GLL grid with four spectral elements of order 10).

same in all the variables for the simulations. In Fig. 5, three grids that were used in the simulation are shown. The p-convergence rates of the H^0 and H^1 error norms are displayed as functions of the polynomial order N in Figs. 6 and 7, respectively.

It can clearly be observed in Fig. 6 that the H^0 error norms of all the variables converge at an exponential rate. The result of the V-velocity component is not shown in figures since it yields a convergence rate similar to that yielded by the U-velocity component. Figures 6a and 7a reveal that the U-velocity components of all test cases converge at approximately the same p-convergence rate (e.g., all the lines fall on top of each other). The H^0 and H^1 error

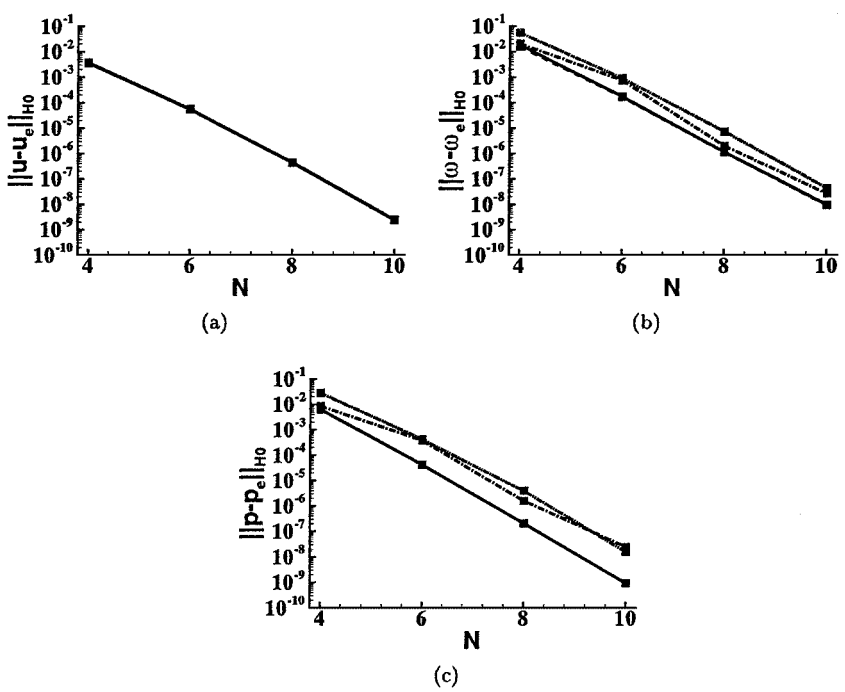

FIG. 6. The p-convergence rate of the H^0 error norms for the various test cases (Bc 2: -; Overdet. Bc: - -; Bc 5a: ---; and Bc 5b: ----).

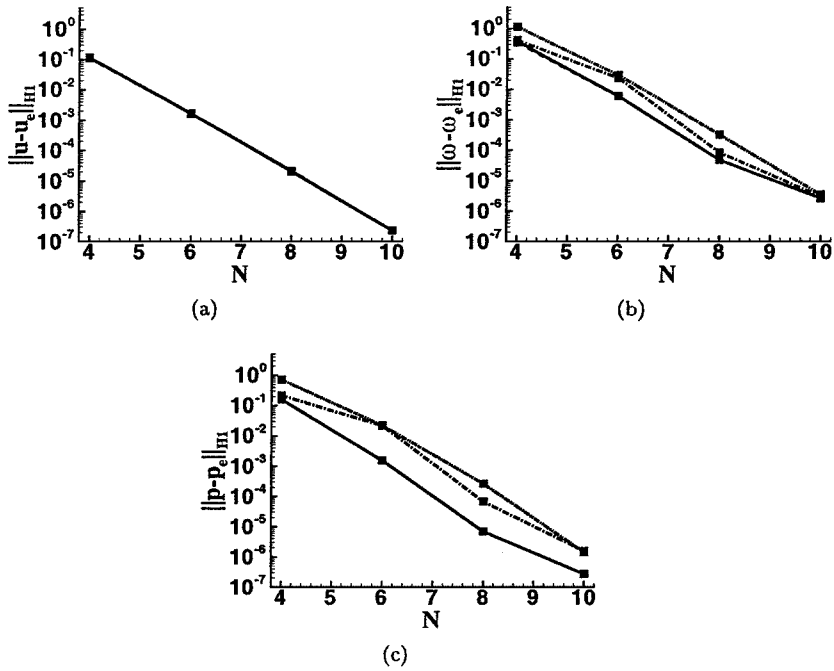

FIG. 7. The p-convergence rate of the H^1 error norms for the various test cases (Bc 2: -; Overdet. Bc: - -; Bc 5a: ---; and Bc 5b: ----).

norms of the vorticity and pressure show that all the test cases converge at approximately the same rate. Comparison of the H^0 error norms of formulation 5a (nonweighted formulation) and 5b (weighted formulation) with those of the other test cases indicates that weighting has a positive effect on the smoothness of the p-convergence rates but leads to slightly less accurate results. Notice that both test cases with velocity boundary conditions give rise to slightly less accurate results for the vorticity and pressure variable. The H^1 error norms of the vorticity and pressure show more scatter in the data.

From these results one can safely conclude that the H^0 and H^1 error norms of all variables demonstrate spectral accuracy. A careful inspection of the p-convergence rates further revealed that prescribing the pressure on the boundary (the fully H^1-coercive formulations) leads to a pressure accuracy which is half an order of magnitude better than the accuracy of the velocity components for larger values of $N(N \geq 6)$. When the pressure was not prescribed on the boundary, the velocity was one order of magnitude more accurate than the pressure and vorticity. All the results indicate that the test case with the overdetermined but consistent boundary conditions can also be considered a fully H^1-coercive formulation since it always displayed the best results (e.g., the results obtained with the overdetermined boundary condition always lie on top of the results obtained with the inflow boundary condition). Moreover, since we did not experience a dramatic loss of accuracy for the non fully H^1-coercive formulations, we believe that the development of spectral element methods based on least-squares formulations is worth continuing in the future. An example of the difference in accuracy between h-refinement and p-refinement is shown in Fig. 8. The results are obtained for the inflow boundary condition and are typical for all the test cases and show the advantage of the use of higher order methods for smooth problems.

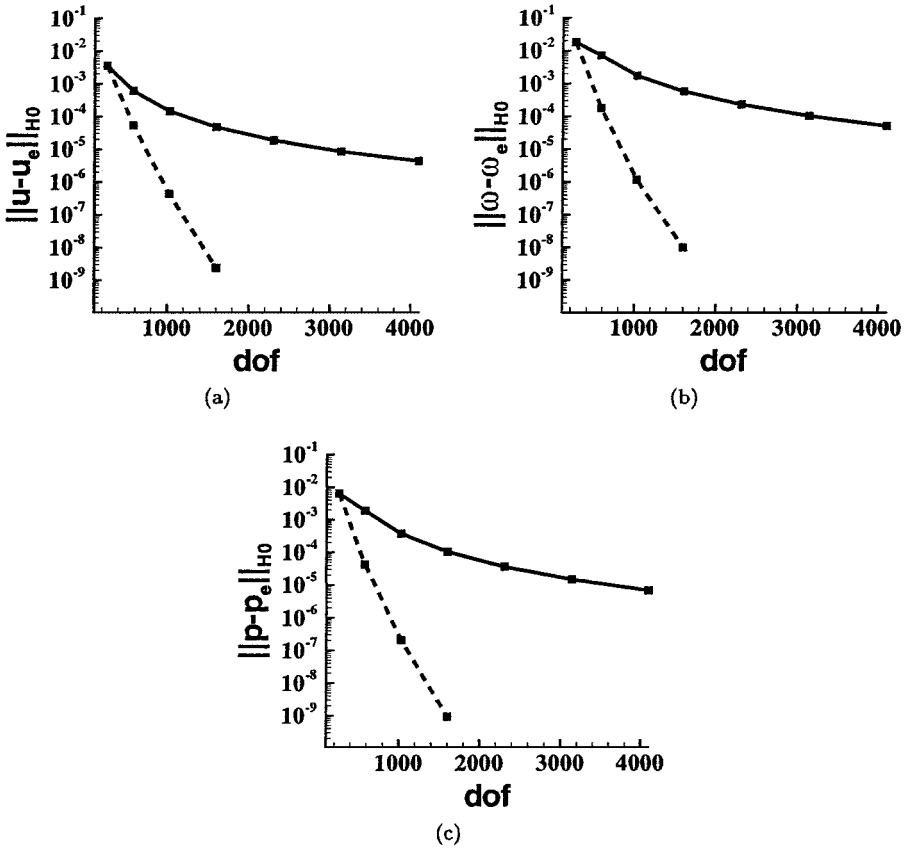

FIG. 8. The h-versus p-convergence rates of the H^0 error norms obtained with the homogeneous inflow boundary condition (h-convergence rate: -; p-convergence rate: - -).

5.5. Comparison with the Galerkin Spectral Element Method

In this section a comparison is made with the Galerkin spectral element method in terms of the h- and p-convergence rates of the H^0 error norms. The smooth model problem supplemented with the velocity boundary conditions is therefore solved with the commonly used Galerkin spectral element method [14, 25]. To this end, the $P_N \times P_{N-2}$ formulation of Bernardi and Maday [4], [26] is used to obtain the discretized Stokes equations.

In what follows, the h- and p-convergence rates of the H^0 error norms obtained with the Galerkin formulation will be compared with the convergence rates obtained with the non-weighted (5a) and weighted (5b) least-squares formulation since these three formulations can be used in conjunction with the velocity boundary conditions. The number of spectral elements (K) and the polynomial order (N) that have been used for the Galerkin simulation are the same as those used for the least-squares formulation. The h-convergence rates of the H^0 error norms are displayed as a function of the grid parameter h in Figs. 9a to 9c. The p-convergence rates of the H^0 error norms are shown as a function of the polynomial order N in Figs. 10a to 10c, respectively. Since the result of the V-velocity component yields a similar convergence rate as does that of the U-velocity component, it is not discussed.

It can be observed in Fig. 9a that the convergence rate of the U-velocity component is approximately the same for the least-squares and Galerkin formulations. Comparing the

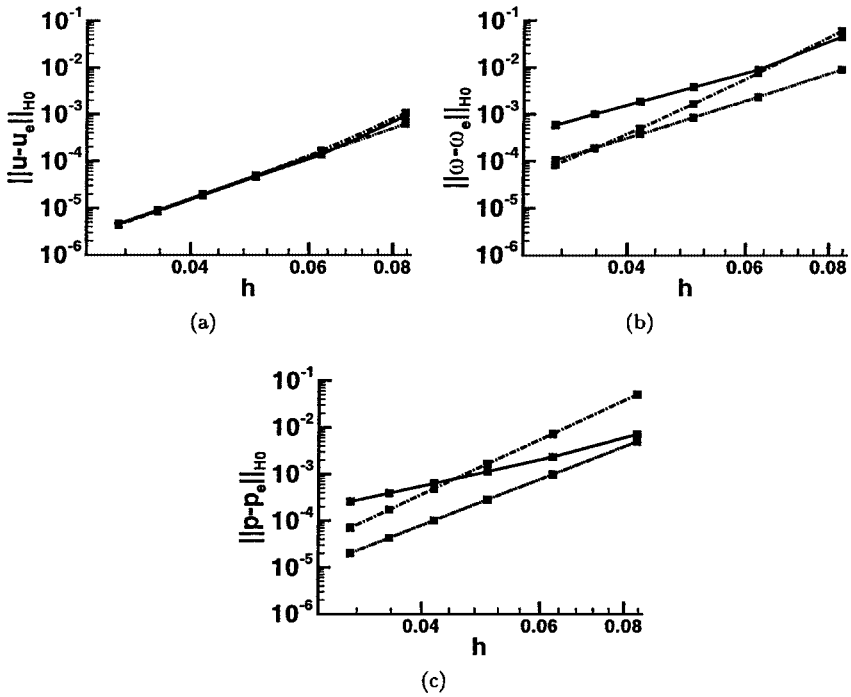

FIG. 9. The h-convergence rate of the H^0 error norms for the least-squares formulation and Galerkin formulation. (Galerkin formulation: -, least-squares formulation 5a: ·--; and least-squares formulation 5b: ·---).

h-convergence rate of the vorticity (Fig. 9b) reveals that the nonweighted least-squares formulation (5a) has approximately the same order of accuracy as the Galerkin formulation at high values of h but has a higher h-convergence rate. This least-squares formulation recovers, at small values of h, the same accuracy as the weighted least-squares formulation (5b) and is roughly one order of magnitude more accurate than the Galerkin spectral element formulation. Comparing least-squares formulation (5b) with the Galerkin formulation reveals that both formulations have approximately the same convergence rate, but this least-squares formulation is, over the whole range of h values, one order of magnitude more accurate than the Galerkin formulation. The difference between the least-squares and the Galerkin formulation is due to the fact that the vorticity needs to be derived from the velocity components in the Galerkin formulation. Comparing the h-convergence rate of the U-velocity component and the vorticity of the Galerkin formulation indicates that one loses approximately one and a half orders of accuracy by calculating the vorticity from the velocity components. In Fig. 9c, the h-convergence rates of the pressure are shown. This figure further reveals that the weighted least-squares formulation (5b) is more accurate than the Galerkin formulation, in particular at smaller values of the grid parameter h. The nonweighted least-squares formulation is only more accurate for small values of h.

The p-convergence rate for the U-velocity component (see Fig. 10a) shows similar convergence behaviour of the least-square method and the Galerkin method. We have no explanation for the surprising result of the Galerkin method at $N = 10$. In Fig. 10b, the p-convergence rates of the vorticity are shown. From this figure, it can clearly be observed that both least-squares formulations (5a and 5b) remain roughly one order of magnitude more accurate than the Galerkin formulation. On the contrary, the accuracy of the pressure

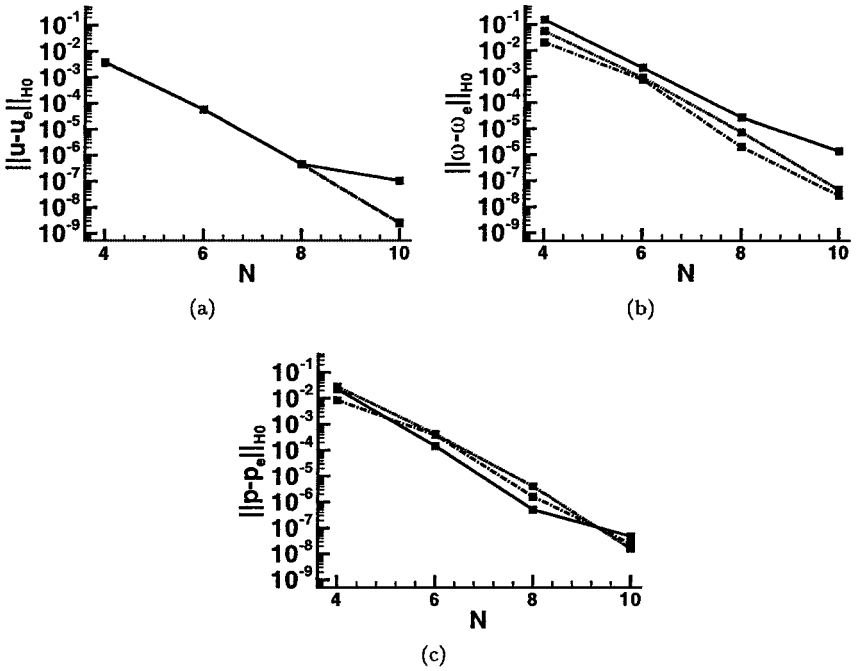

FIG. 10. The p-convergence rate of the H^0 error norms for the least-squares formulation and the Galerkin formulation. (Galerkin formulation: -; least-squares formulation 5a: - · -; and least-squares formulation 5b: -·--).

variable (see Fig. 10c) seems approximately one order of magnitude more accurate when the Galerkin formulation is used instead of the least-squares formulation. This superior behaviour is lost at $N = 10$. At this polynomial order, the Galerkin formulation becomes less accurate than the least-squares formulations. This is probably due to the fact that the velocity was also substantially less accurate at this polynomial order (see Fig. 10a).

The results of the present smooth model problem seem to indicate that the least-squares spectral element method and the Galerkin spectral element method yield comparable results regarding the accuracy of the velocity components. Moreover, the accuracy of the vorticity variable obtained with least-squares spectral element methods is one order of magnitude higher than the results obtained with the Galerkin method. When the pressure variable is considered, the Galerkin method seems more accurate, at least when p-refinement is used. On the whole, least-squares spectral element methods seem to provide the same order of accuracy as the more commonly used Galerkin spectral element methods for this smooth model problem.

The main advantages of using the least-squares method instead of the Galerkin method to solve the incompressible Stokes and Navier–Stokes equations is that least-squares methods lead to symmetric systems regardless of the underlying partial differential equations (also when a Newton linearization would have been used). It has been shown in [6] that the incompressible Stokes and Navier–Stokes equations also yield postive definite algebraic systems and circumvent the LBB stability condition. Moreover, these systems can be solved with robust iterative methods such as the preconditioned conjugate gradient method and additive and multiplicative multigrid methods [2, 7, 8]. In contrast, the Galerkin method yields a saddle point problem which is more difficult to solve numerically. To overcome

this drawback, the discrete governing equations are often uncoupled by using projection methods or generalized block LU-decompositions.

The application of the least-squares method to some more demanding problems such as the cylinder problem [12] revealed that the major disadvantage of the least-squares method is the mass conservation property. Numerical experience (not discussed here) revealed that the present least-squares spectral element method performs much better than the least-squares finite element method used in [12] and that a suitable weighting of the continuity equation (see [15]) in the least-squares functional almost restores mass conservation. A way to restore the mass conservation in the least-squares spectral element formulation of the Stokes problem will be discussed in forthcoming work [26a, 26c].

6. CONCLUSIONS

In the present paper, a least-squares spectral element method for the Stokes equations has been discussed. Least-squares spectral element methods are based on two important and successful numerical methods which are spectral/hp element methods and least-squares finite element methods. In this respect, least-squares spectral element methods seem the best of all worlds since they combine the generality of finite element methods with the accuracy of the spectral methods. There are also theoretical and computational advantages in the algorithmic design and implementation of the least-squares methods. Most notably, least-squares methods lead to symmetric and positive definite algebraic systems which circumvent the Ladyzhenskaya–Babuška–Brezzi stability condition and consequently allow the use of equal-order interpolation polynomials for all the variables.

These three feature—high accuracy, equal-order interpolation, and systems which are easy to solve—make the proposed method a competitive candidate for the solution of large-scale problems arising in scientific computing. In order to demonstrate its competitiveness, the method has been applied to an analytical problem and the theoretical optimal and suboptimal a priori estimates have been confirmed for various boundary conditions or, equivalently, various approximating function spaces. Most notably, the use of wall boundary conditions (boundary conditions 5), i.e., the prescription of the normal and tangential velocity components, leads to optimal h-convergence rates for the velocity components. Suboptimal results in the vorticity, as was to be expected, were found. The h-convergence rates for the pressure were much better than expected. Further experiments with least-squares spectral element methods will, we hope, clarify whether this phenomenon is model problem dependent or a general trend for higher order methods. The comparison with the Galerkin spectral element method revealed that the method is equally as accurate as the Galerkin formulation and even superior when the other boundary conditions are employed. The overdetermined but consistent boundary condition also yields optimal accurate results. The p-convergence rates of the least-squares spectral element formulation of the Stokes problem revealed that the choice of the boundary condition has no effect on the exponential p-convergence behaviour. Moreover, the results revealed that the use of the inflow and overdetermined boundary condition leads to a pressure accuracy which is slightly better than the accuracy of the velocity components for high spectral element orders. When the pressure was not prescribed on the boundary, the accuracy of the velocity components was one order more accurate than the pressure and vorticity.

Since we did not experience any dramatic loss of accuracy when h- or p-refinement was applied in any of our test cases, we believe that spectral element methods based on

least-squares formulations might be good candidates for use in developing new hp-adaptive strategies for future generation large-scale (Navier–Stokes) solvers.

ACKNOWLEDGMENT

The authors are pleased to acknowledge the constructive suggestions and comments of professor B.-N. Jiang.

REFERENCES

1. S. Agmon, A. Douglis, and L. Nirenberg, Estimates near the boundary for solutions of elliptic partial differential equations satisfying general boundary conditions ii, *Commun. Pure Appl. Math.* **17**, 35 (1964).
2. D. N. Arnold, R. S. Falk, and R. Winther, Preconditioning in $H(div)$ and applications, *Math. Comput.* **66**(219), 957 (1997).
3. A. K. Aziz, R. B. Kellogg, and A. B. Stephens, Least-squares methods for elliptic systems, *Math. Comput.* **44**(169), 53 (1985).
4. C. Bernardi and Y. Maday, *Approximations Spectrale de Problèmes aux Limites Élliptiques* (Springer-Verlag, Berlin/New York, 1992).
5. P. B. Bochev and M. D. Gunzburger, Analysis of least squares finite element methods for the Stokes equations, *Math. Comput.* **63**(208), 479 (1994).
6. P. B. Bochey and M. D. Gunzburger, Finite element methods of least-squares type, *SIAM Rev.* **40**(4), 789 (1998).
7. Z. Cai, R. Lazarov, T. A. Manteuffel, and S. F. McCormick, First-order system least-squares for second-order partial differential equations, *SIAM J. Numer. Anal.* **31**(6), 1785 (1994).
8. Z. Cai, T. A. Manteuffel, and S. F. McCormick, First-order system least-squares for the Stokes equations, with application to linear elasticity, *SIAM J. Numer. Anal.* **34**(5), 1727 (1997).
9. G. F. Carey and B.-N. Jiang, Element-by-element linear and nonlinear solution schemes, *Commun. Appl. Numer. Meth.* **2**, 145 (1986).
10. G. F. Carey and B.-N. Jiang, Least-squares finite element method and preconditioned conjugate gradient solution, *Int. J. Numer. Meth. Eng.* **24**, 1283 (1987).
11. G. F. Carey, Y. Shen, and R. T. Mclay, Parallel conjugate gradient performance for least-squares finite elements and transport problems, *Int. J. Numer. Meth. Fluids* **28**, 1421 (1998).
12. C. L. Chang and J. J. Nelson, Least-squares finite element method for the Stokes problem with zero residual of mass conservation, *SIAM J. Numer. Anal.* **34**(2), 480 (1997).
13. P. G. Ciarlet, *Finite Element Methods for Elliptic Problems* (North Holland, Amsterdam, 1998), Vol. 4.
14. W. Couzy, *Spectral Element Discretization of the Unsteady Navier–Stokes Equations and its Iterative Solution on Parallel Computers*, Ph.D. thesis (Ecole Polytechnique Fédérale de Lausanne, 1995).
15. J. M. Deang and M. D. Gunzburger, Issues related to least-squares finite element methods for the Stokes equations, *SIAM J. Sci. Comput.* **20**(3), 878 (1998).
16. X. Ding and T. T. H. Tsang, Large eddy simulation of turbulent flows by a least-squares finite element method, *Int. J. Numer. Meth. Fluids* **37**, 297 (2001).
17. M. I. Gerritsma and T. N. Phillips, Discontinuous spectral element approximations for the velocity-pressure-stress formulation of the Stokes problem, *Int. J. Numer. Meth. Eng.* **43**, 1401 (1998).

17a. M. I. Gerritsma and M. M. J. Proot, Analysis of a discontinous least-squares spectral element method, *J. Sci. Comput.* **17**(1–3), 323 (2002).

18. R. D. Henderson, Adaptive spectral element methods for turbulence and transition, in *Higher Order Discretization Methods for Computational Physics*, edited by T. J. Barth and H. Decomimck (Springer-Verlag, New York/Berlin, 1999), pp. 225–324.
19. C. Hirsch, *Numerical Computation of Internal and External Flows* (Wiley, New York, 1988).
20. B.-N. Jiang, A least-squares finite element method for incompressible Navier-Stokes problems. *Int. J. Numer. Meth. Fluids* **14**, 843 (1992).

21. B.-N. Jiang, *The Least-Squares Finite Element Method* (Springer-Verlag, Berlin/New York, 1998).
22. B.-N. Jiang, On the least-squares method, *Comput. Meth. Appl. Mech. Eng.* **152**, 239 (1998).
23. B.-N. Jiang and C. L. Chang, Least-squares finite elements for the Stokes problem, *Comput. Meth. Appl. Mech. Eng.* **78**, 297 (1990).
24. B.-N. Jiang and L. Povinelli, Least-squares finite element method for fluid dynamics, *Comput. Meth. Appl. Mech. Eng.* **81**(1), 13 (1990).
25. G. E. Karniadakis and S. J. Sherwin, *Spectral/hp Element Methods for CFD* (Oxford Univ. Press, London, 1999).
26. Y. Maday and A. T. Patera, Spectral element methods for the incompressible Navier-Stokes equations, in *State-of-the-Art Surveys on Computational Mechanics*, edited by A. K. Noor and J. T. Oden (Am. Soc. Mech. Eng., 1989).
26a. M. M. J. Proot, The development of least-squares spectral element methods for incompressible flow problems, Ph.D. thesis (Delft University of Technology, 2003).
26b. M. M. J. Proot and M. I. Gerritsma, A least-squares spectral element formulation for the Stokes problem, *J. Sci. Comput.* **17**(1–3), 311 (2002).
26c. M. M. J. Proot and M. I. Gerritsma, Mass conservation of least-squares methods: Revisited, in preparation.
27. A. Quateroni and A. Valli, *Numerical Approximation of Partial Differential Equations* (Springer-Verlag, Berlin/New York, 1997).